

# Bio-inspired functional surfaces for migration-lubrication control under external thermal gradients

Hao Qiu<sup>a,b</sup>, Qingwen Dai<sup>a,b,\*</sup>, Wei Huang<sup>a,b</sup>, Xiaolei Wang<sup>a,b</sup>

<sup>a</sup> National Key Laboratory of Helicopter Aeromechanics, Nanjing University of Aeronautics and Astronautics, Nanjing 210016, China

<sup>b</sup> College of Mechanical and Electrical Engineering, Nanjing University of Aeronautics and Astronautics, Nanjing 210016, China

## ARTICLE INFO

### Keywords:

Bionic surface texture  
Migration  
Lubrication  
Interface phenomenon

## ABSTRACT

In this work, a bio-inspired surface texture was developed to regulate lubricant migration and interfacial lubrication. Reciprocating friction tests in horizontal and vertical orientations were conducted to examine how thermal gradients and gravity influence the lubrication behavior of textured surfaces. Results demonstrated that surface texturing can effectively reduce friction and control lubricant loss under different directional forces. In simulated point-to-plane contact of the rotating pair tests under low-speed, light-load rotation, the textures enhanced resistance to centrifugal effects and improved lubrication stability. These findings confirm the potential of biomimetic surface designs for improving point-to-plane lubrication in complex operating conditions, with promising applications in aerospace bearings and precision motion systems.

## 1. Introduction

With the development of modern industrial technologies, particularly in aerospace and precision instrumentation, the reliability of lubrication systems has become increasingly critical. Insufficient lubricant supply leads to direct contact at friction interfaces, resulting in an elevated coefficient of friction (COF), accelerated wear, and potential mechanical failure. Major contributing factors include mechanical vibration [1], centrifugal and electromagnetic forces [2], and thermocapillary effects [3,4]. Among these, thermally induced lubricant migration is particularly significant, as it critically limits the service life and reliability of mechanical systems. Thermal capillary migration refers to the spontaneous transport of lubricants from high- to low-temperature regions at frictional interfaces, driven by surface tension gradients induced by temperature differentials [5,6]. Regarding thermal capillary migration, investigations have focused on temperature gradients and surface tension effects. Dai et al. [7,8] analyzed droplet dynamics and micro-dimple textures for lubricant control. Grützmacher et al. [9,10] further demonstrated the guiding effect of micro-groove arrays on lubricant migration under thermal gradients. Collectively, these studies provide a theoretical foundation for controlling solid-liquid interfacial behavior in thermally complex environments.

In recent years, biomimetic surface technologies have demonstrated considerable potential for addressing lubrication-related challenges.

Among various structural designs, wedge-shaped geometries [11] have attracted particular interest due to their ability to induce spontaneous liquid transport via Laplace pressure gradients arising from curvature variations [12–17]. To address this technical challenge, researchers have drawn significant inspiration from nature, where biological organisms exhibit sophisticated strategies for liquid manipulation [18]. Many natural structures possess the ability to guide and regulate liquid transport in a highly controlled manner [19–23]. For instance, cactus spines and spider silk utilize surface microstructures to induce Laplace pressure gradients and surface energy gradients, thereby enabling efficient water harvesting [18,24,25]. The surface of rice leaves features a unique sinusoidal groove structure that effectively guides the directional movement of droplets [26,27]. Similarly, *Nepenthes* utilizes a spontaneous droplet transport mechanism to continuously deliver water to the periphery of its pitcher, maintaining surface wettability essential for effective prey capture [28]. These intricate natural designs have inspired the development of functional artificial surfaces for tribological applications. Zhang et al. [29] designed a fishbone-like texture that reduced friction by 63.3 %. Dai et al. [30] constructed wedge-grooved surfaces for directional lubricant transport. Guo et al. [31] proposed comb-like textures to enhance film thickness and reduce bearing friction. Vidyasagar et al. [32] reported performance improvements in deep groove ball bearings by integrating bionic textures on the inner race. Pattanayak et al. [33] demonstrated that combining bionic textures with

\* Correspondence to: Yudao street 29#, Nanjing, China.

E-mail address: [daiqingwen@nuaa.edu.cn](mailto:daiqingwen@nuaa.edu.cn) (Q. Dai).

<https://doi.org/10.1016/j.triboint.2025.111039>

Received 22 May 2025; Received in revised form 22 July 2025; Accepted 26 July 2025

Available online 28 July 2025

0301-679X/© 2025 Elsevier Ltd. All rights are reserved, including those for text and data mining, AI training, and similar technologies.

micro-pockets enhanced the oil film stability in journal bearings. Gouda et al. [34–37] studied the fatigue life, vibration response, and tribodynamic behavior of ball bearings with micro-grooved inner or outer races under both dry and lubricated conditions.

The existing literature has provided valuable insights into the bio-inspired functional surfaces. However, when considering the thermal capillary migration in real applications, several critical challenges remain unresolved. Few studies have considered the influence of gravity, and a systematic understanding of thermal capillary migration under coupled conditions of temperature gradients and complex motion states, such as vertical and rotational movements, is still lacking. Furthermore, the long-term stability and reliability of existing surface textures require further enhancement. Addressing these issues is essential for the development of next-generation space lubrication technologies.

Hence, this study focuses on point-to-plane friction pairs and proposes a V-shaped array texture inspired by the structure of *Metasequoia* leaves. By adjusting the inclination angle of the texture elements, multiple texture configurations were achieved. The structure generates multiple localized Laplace pressure gradients that drive liquid transport toward the center through converging pathways, presenting a distinct contrast to conventional single-wedge designs [38] and offering a novel strategy for active lubricant regulation. The lubrication regulation mechanisms of surface textures under multi-field coupling of temperature gradient and gravity were systematically investigated in both horizontal and vertical directions. Moreover, the influence of texture inclination parameters on lubricant transport performance was analyzed. Furthermore, low-speed and light-load rotational conditions of point-to-plane contact of the rotating pair were simulated to explore the effects of texture arrangement direction on lubrication performance. The findings provide important insights for improving the lubrication efficiency and durability of mechanical friction pairs.

## 2. Experiment

### 2.1. Materials

In this work, lubrication and migration experiments were carried out based on the point-to-plane contact pair. The upper specimen consisted of a silicon nitride  $\text{Si}_3\text{N}_4$ -ball (10 mm diameter, surface roughness

(Ra):20–50 nm, NSK, China), which exhibits enhanced friction and wear compatibility with metallic counterparts under reciprocating wear conditions [39]. The lower specimen was an aluminum plate (1090,  $\text{Al} \geq 99.95\%$ , 70 mm × 20 mm × 3 mm, surface roughness (Ra):20–150 nm, Hefei Wenghe Metal Materials Co., Ltd., China), due to its excellent thermal conductivity and machinability [40]. Poly- $\alpha$ -olefin (PAO4, kinematic viscosity (40 °C):19.42  $\text{mm}^2/\text{s}$ , density (20 °C):817.9  $\text{kg}/\text{m}^3$ ) synthetic base oil (Shenzhen Huashengyuan Petrochemical Technology Co., Ltd., China) served as the lubricant. PAO4 was chosen for its optimal rheological properties, featuring a low kinematic viscosity and excellent flow characteristics at both ambient and elevated temperatures [31]. Compared to conventional mineral oils, this synthetic hydrocarbon exhibits superior oxidation stability and viscosity–temperature performance, making it particularly suitable for high-performance rolling bearings in precision equipment.

### 2.2. Design of bio-inspired functional surfaces (BMLB)

The functional surfaces were inspired by the *metasequoia* leaf-blade (Bionic *metasequoia* leaf blade, BMLB) pattern, as shown in Fig. 1(a). The central main groove resembles the midrib structure connected to the petiole, with lanceolate, leaf-like units distributed along both sides, forming a radially arranged V-shaped array.

The fabrication process is illustrated in Fig. 1(b). First, the polished and cleaned aluminum sample was subjected to electrochemical treatment for 7 min at a current density of 0.7  $\text{A}/\text{cm}^2$ , followed by cleaning and drying to obtain an irregular stepped micro-rough morphology. Subsequently, the electrochemically treated aluminum sample was boiled in deionized water for 40 min to further roughen the surface. The boiled sample was then immersed in a 0.02 mol/L solution of 1H,1H,2H,2H-Perfluorodecyltrichlorosilane (PFDTs) in anhydrous ethanol for 3 h. After chemical treatment, the sample was dried in a vacuum oven at 176 K with a vacuum level of  $-0.1$  kPa for 15 min to achieve a low-surface-energy surface (Rough surface). Finally, the texture patterning was performed using a laser marking system (JPT Seal-355-5, China). Ensuring that the texture possesses reliable and stable surface functionality while preventing lubricant accumulation that could diminish lubrication efficiency. The laser parameters were set at 3.5 W power, 40 kHz frequency, and 1500 mm/s scanning speed,

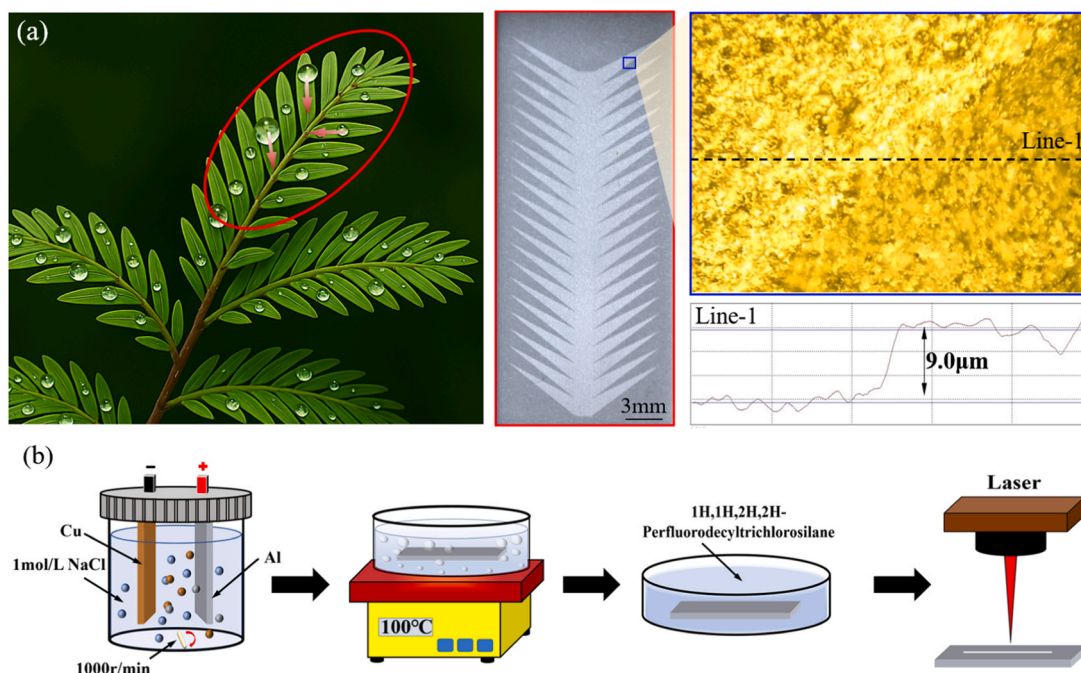


Fig. 1. BMLB texture source and fabrication process (a) Diagram of the BMLB texture configuration (b) Texture fabrication process.

producing textures with a depth of 8–10  $\mu\text{m}$  [29–31] as shown in Fig. 1 (a).

Based on the angle  $\alpha$  relative to the vertical direction, three types of textures were designed: Bionic metasequoia leaf blade  $0^\circ$  texture (BMLB- $0^\circ$ ), Bionic metasequoia leaf blade  $5^\circ$  texture (BMLB- $5^\circ$ ), and Bionic metasequoia leaf blade  $30^\circ$  texture (BMLB- $30^\circ$ ). Detailed parameters are summarized in Table 1.

The laser-scanned surface without patterning is called Laser surface. This process resulted in an oil-phobic texture interior and superoleophobic exterior, with various oils exhibiting contact angles greater than  $130^\circ$  on the exterior and less than  $10^\circ$  on the interior of the textures, as shown in Fig. 2.

### 2.3. Experiment apparatus

The tests were conducted using a self-constructed surface tribology mechanics testing platform, as shown in Fig. 3(a). The surface tribology mechanics testing platform was capable of generating both horizontal and vertical temperature gradients to investigate the effects of thermally induced directional variations on oil lubrication performance. The thermal gradients were established using MCH high-temperature ceramic heaters ( $0\text{--}200^\circ\text{C}$ , 24 V, 40 W, China) and a water-circulating chiller ( $0.5^\circ\text{C}\text{--}25^\circ\text{C}$ ) to establish controlled temperature differentials across the solid specimen surface. Temperature regulation was implemented through K-type precision thermocouples ( $-40\text{--}260^\circ\text{C}$ ) coupled with a REX-C100 universal digital temperature controller (YTG-850W, China). Frictional force measurements were conducted via a quadrilateral cantilever beam system incorporating laser displacement sensors and double-layer spring plates, a normal load ranging from 0 to 100 mN could be applied and enabling millinewton-level precision during

contact interactions.

### 2.4. Experimental process

To evaluate the creep-lubrication regulation performance of textured surfaces on lubricant behavior, a series of experiments were conducted under both horizontal (without gravity) and vertical (with gravity) orientations, as detailed below.

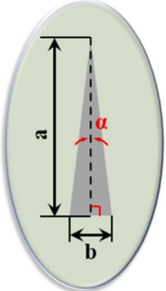
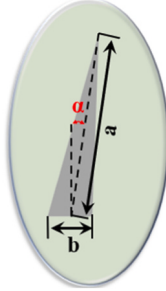
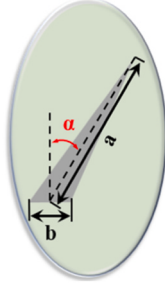
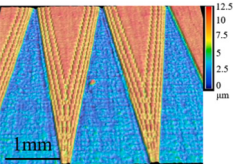
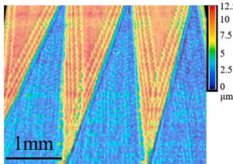
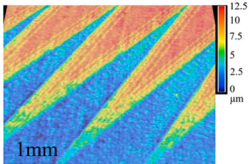
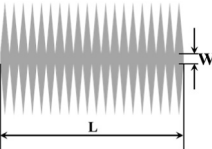
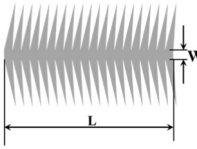
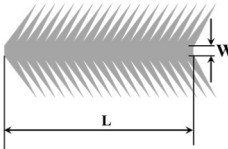
#### 2.4.1. Horizontal friction test

As shown in Fig. 3(b), the upper  $\text{Si}_3\text{N}_4$ -ball sample was fixed at the end of a cantilever beam, while the lower aluminum plate sample was mounted on a load displacement platform. The platform moved reciprocally at a speed of  $50\text{ }\mu\text{m/s}$  over a distance of 10 mm, with a preload of 50 mN applied as the normal load to ensure effective contact between the upper and lower samples. The reciprocating friction test is conducted sequentially on aluminum and electrolyzed surfaces under dry conditions, with  $3\text{ }\mu\text{L}$  of PAO4 oil lubrication, after the introduction of a temperature gradient with PAO4 lubrication, and with the addition of three types of textures. The temperature conditions were set with the hot end at  $115^\circ\text{C}$  and the cold end at  $5^\circ\text{C}$ , with a distance of 40 mm, resulting in a stable temperature gradient of  $2.75^\circ\text{C/mm}$ . Each reciprocating motion constituted one cycle, and a total of 5 continuous cycles were performed.

#### 2.4.2. Vertical friction test

As shown in Fig. 3(c), to further investigate the effect of gravity, the lower aluminum plate sample was placed vertically, and the upper  $\text{Si}_3\text{N}_4$ -ball sample was rotated  $90^\circ$  to make contact with it. The preload was increased to 100 mN to reduce the amplitude of fluctuations in the

**Table 1**  
Texture design parameters.

Name	BMLB- $0^\circ$	BMLB- $5^\circ$	BMLB- $30^\circ$
Inclination angle	$\alpha = 0^\circ$	$\alpha = 5^\circ$	$\alpha = 30^\circ$
Unit			
3D morphology			
Array structure			
Area Density	54.84 %	53.67 %	50.19 %
Groove length	$L = 30\text{ mm}$		
Groove width	$W = 1.5\text{ mm}$		
Texture width	$b = 1.5\text{ mm}$		
Centerline length	$a = 7\text{ mm}$		

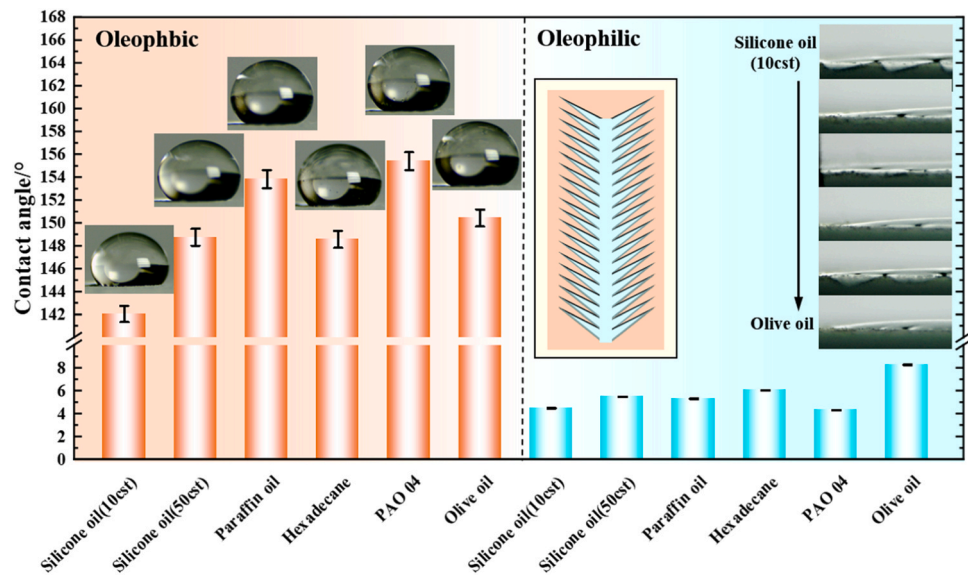


Fig. 2. Contact angle of lubricant on textured surface.

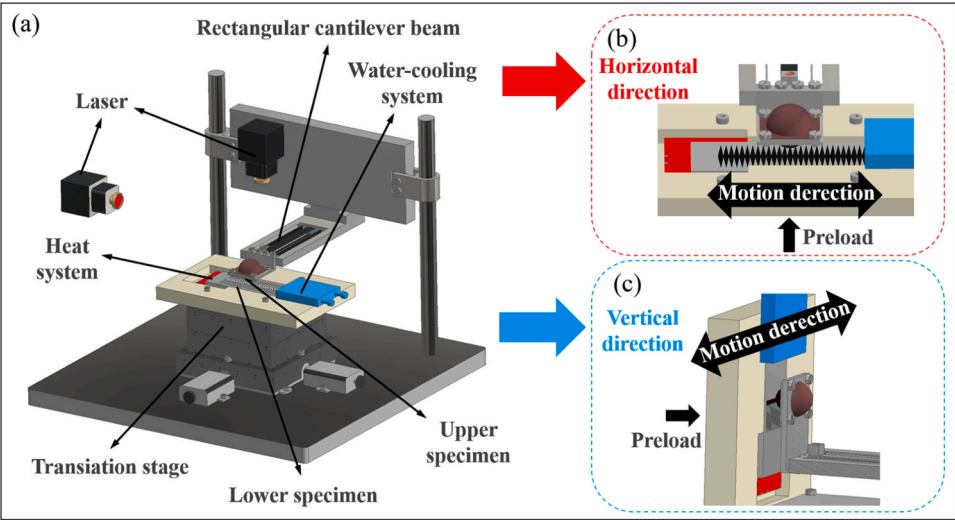


Fig. 3. (a) Self-constructed surface tribology mechanics testing platform (b) Horizontal test (c) Vertical test.

Table 2  
Test condition parameters.

Parameters		Horizontal direction	Vertical direction
Orientation	Gravity, $G$ Thermal gradient, $\Delta T$ Moving velocity, $V$		
Experimental conditions	Load Temperature setting Velocity Displacement Lubrication condition	50 mN 2.75 °C/mm (hot 115 °C , cold 5 °C) 50 μm/s 10 mm PAO4 (3 μL)	100 mN



cantilever spring beam. The dry friction tests on aluminum and electrolyzed surfaces were omitted in this configuration. All other conditions were consistent with those of the horizontal direction test. Detailed experimental parameters are provided in Table 2.

### 3. Results and discussion

#### 3.1. Horizontal reciprocating friction test

The experimental results are shown in Fig. 4(a). As can be seen, the rough surface (with superhydrophobic treatment, without texture) exhibits the highest surface roughness and COF, consistent with expectations for hydrophobic/oil-repellent surfaces produced by the electrolytic method. And laser surface (without texture) lowers the COF, indicating that wettability control improves frictional behavior. The addition of PAO4 lubricant significantly reduces the COF, but after the 4th cycle, the lubricant in the contact area gradually depletes, leading to lubricant depletion and rising COF, especially under a temperature gradient, which accelerates lubricant migration and failure. Surface texturing further reduces COF and improves lubrication durability. During the five reciprocating friction cycles, the textured surface does not exhibit significant increases in COF, demonstrating that surface textures can effectively maintain the stability of the lubricating oil film. As shown in Fig. 4(b), the BMLB-5° textured aluminum surface achieves the lowest

average COF and minimal fluctuations, confirming the tribological benefits of biomimetic texture design. It is evident that, compared to without-textured surface, the BMLB surface achieves a reduction in average COF by more than 31 %.

To further understand the underlying reasons for the observed phenomena, the oil transport capability of textures with different inclination angles is analyzed. As shown in Fig. 5(d), the lubricant within the texture is primarily influenced by the capillary driving force  $F_{cap}$  and the frictional resistance  $F_f$ . The expression for these forces can be written as:

$$F = F_{cap} - F_f \quad (1)$$

Where  $F_{cap}$  represents the capillary driving force, which is mainly induced by the nanoroughness, and  $F_f$  represents the frictional resistance that the lubricant experiences during motion. In the textured channels, the capillary crawling speed can be expressed by the Washburn modified equation as:

$$\frac{dh}{dt} = \frac{r_{eff}\gamma\cos\theta}{4\mu h} - \frac{r_{eff}^2\rho g}{8\mu} \quad (2)$$

Where  $r_{eff}$  represents the equivalent radius, which is determined by the geometric dimensions of the texture (for parallelogram-shaped grooves,  $r_{eff}$  is generally taken as  $L/2$ , where  $L$  is the groove width; two triangular sections can be combined into a parallelogram, so in this case, we take  $r_{eff}=L/4$ ).  $\gamma$  is the surface tension of the liquid,  $\theta$  is the contact average

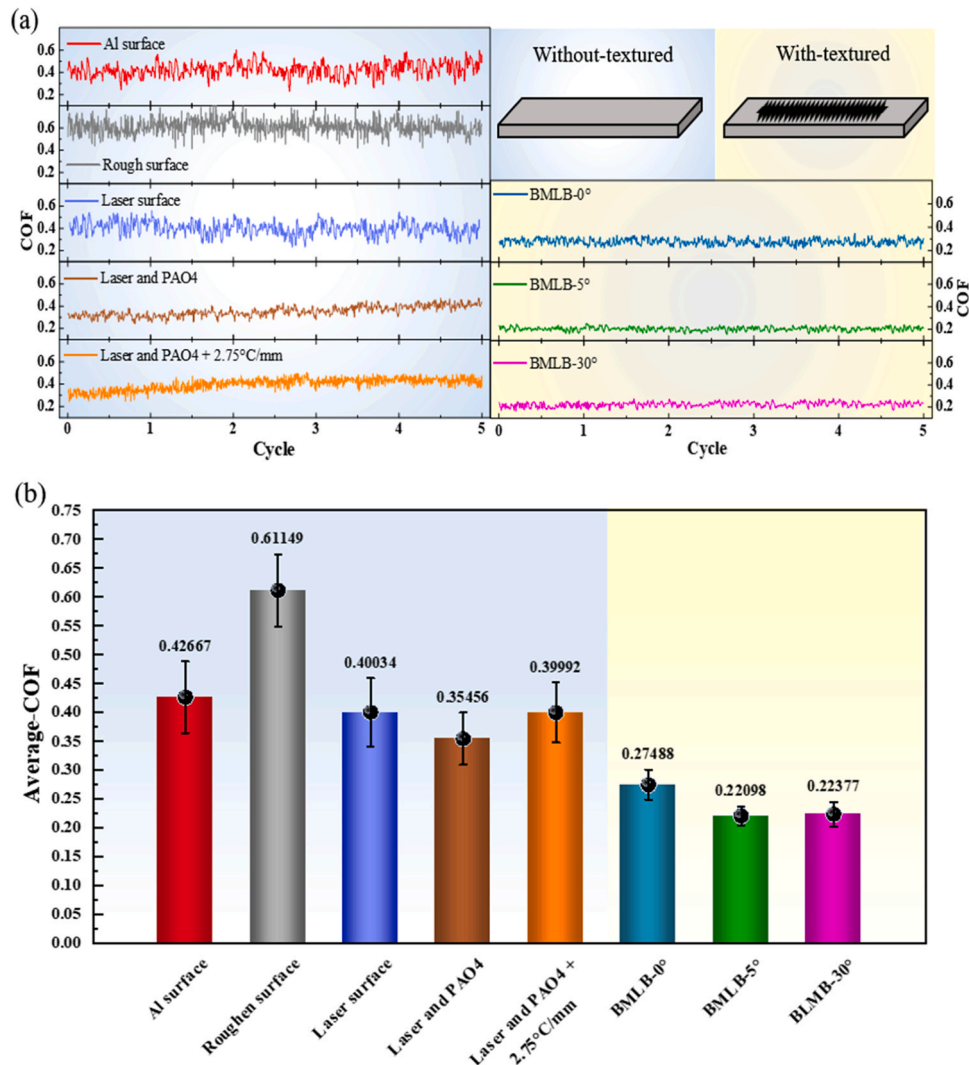
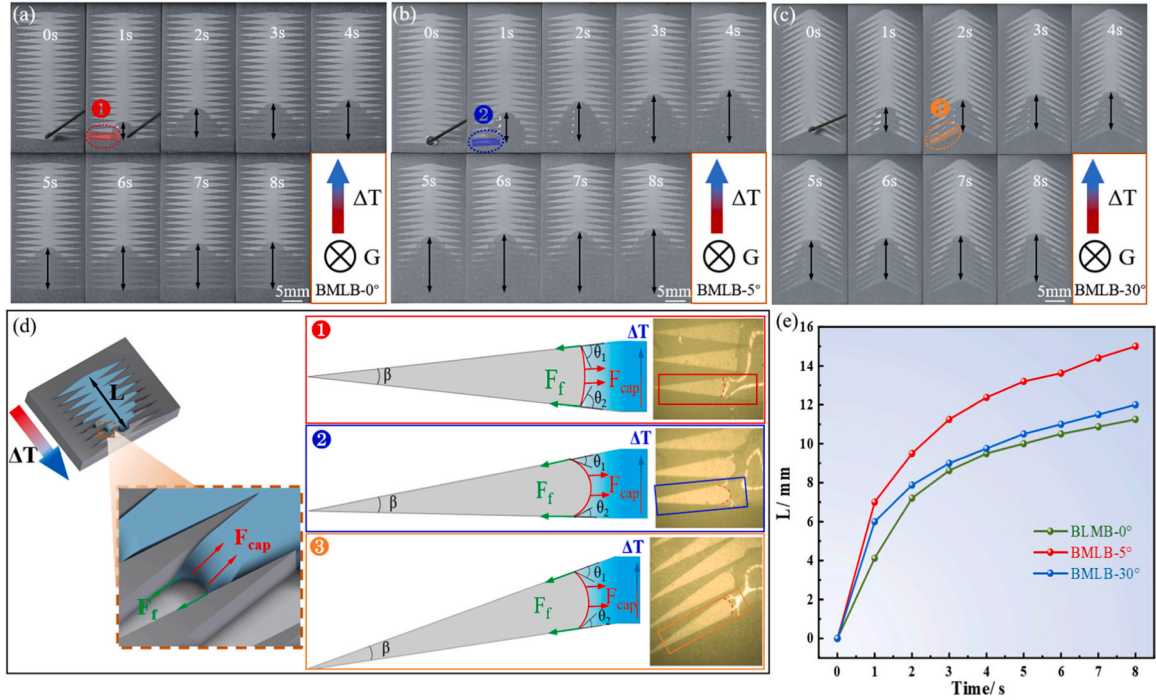


Fig. 4. Horizontal friction test results (a) Without-textured and with-textured COF (b) Average COF.



**Fig. 5.** Lubricant spreading behavior on different textures and force (a) BMLB-0° (b) BMLB-5° (c) BMLB-30° (d) Lubricant force analysis (e) Lubricant spreading distance.

angle formed between the texture and the liquid (Since the contact angles on both sides may differ, we take  $\theta = (\theta_1 + \theta_2)/2$ ),  $\mu$  is the dynamic viscosity of the liquid,  $\rho$  is the density of the liquid,  $g$  is the gravitational acceleration, and  $h$  is the liquid infiltration distance. When equilibrium is reached internally, the capillary force equals the opposing resistance, and the above equation simplifies to:

$$F_{cap} = 2\pi r_{eff} \gamma \cos \theta \quad (3)$$

The frictional resistance  $F_f$  can be divided into two components: fluid viscous friction and texture friction, expressed as:

$$F_f = \tau \cdot A + \mu_{eff} \cdot F_n \cos \frac{\beta}{2} \quad (4)$$

Here,  $\tau$  represents the shear stress,  $A$  is the contact area, and  $\mu_{eff}$  is the effective COF [41–43], which is related to the COF when there is no texture and the efficiency factor. Substituting Eqs. (3) and (4) into Eq. (1) gives the force acting on the lubricant within the texture as:

$$F = 2\pi r_{eff} \gamma \cos \theta - \tau \cdot A - \mu_{eff} \cdot \rho V g \cos \frac{\beta}{2} \quad (5)$$

By observing the lubricant motion under a thermal gradient, as shown in Fig. 5(a)–(c), and analyzing the contact angles within different textures during the first second of movement in Fig. 5(d). It can be seen that, under horizontal placement, the lubricant in the BMLB-5° texture exhibits the smallest contact average angle  $\theta$ , resulting in the maximum driving force. The  $F_f$  increases with decreasing  $\beta$ ; however, the variation in the  $\beta$  angle is relatively small, so the frictional force can be approximated as constant. The lubricant is transported the most toward the center within this texture. Additionally, the surface tension difference  $\Delta\gamma$  generated by the temperature gradient causes the lubricant to flow from the high-temperature region to the low-temperature region. The expression for this can be written as [3]:

$$\Delta\gamma = \left| \frac{d\gamma}{dT} \right| \cdot \Delta T \quad (6)$$

Here,  $\left| \frac{d\gamma}{dT} \right|$  represents the surface tension coefficient (which is related to the type of lubricant), and  $\Delta T$  is the temperature difference. The

distance  $L$  that the lubricant crawls can be expressed as:

$$L \propto V^{1/3} \cdot \Delta T \cdot t \quad (7)$$

The spreading distance of lubricating oil along the temperature gradient is directly proportional to the liquid volume, indicating that the textured surface possesses a certain oil transport capability. A stronger transport capacity corresponds to a larger central lubricant volume and a longer spreading distance under the influence of the temperature gradient. As shown in Fig. 5(e), the oil creep distance within the same time interval is the longest under the BMLB-5° texture, which is consistent with the aforementioned conclusion.

### 3.2. Reciprocating friction test in the vertical direction

As shown in Fig. 6(a), the experimental results demonstrate that the application of PAO4 lubricating oil significantly reduces the COF, indicating effective lubrication performance. However, during vertical reciprocating friction, the influence of gravity facilitates lubricant loss, resulting in a gradual increase in both the COF and its fluctuation amplitude after the second cycle. When a temperature gradient opposite to the direction of gravity is applied, the increasing trend of the COF is partially suppressed, suggesting that the thermal gradient can mitigate lubricant loss to a certain extent. Nevertheless, its effect remains limited and cannot fully counteract gravity-induced oil depletion.

Upon the introduction of surface textures, the COF is further reduced, and a more stable lubrication state is maintained throughout the friction process. Textured surfaces not only exhibit superior friction-reducing capabilities but also effectively delay lubricant loss, thereby enhancing lubrication durability. As shown in Fig. 6(b), a comparison of the average COF under various conditions reveals that the aluminum substrate with BMLB-0° texture performs best, exhibiting the lowest average COF and minimal fluctuation in the friction curve. It can reduce average COF to 34 %. This indicates that the BMLB-0° texture design achieves optimal friction reduction and lubrication stability under vertical reciprocating conditions. Therefore, the BMLB surface oriented in the vertical direction achieves a reduction in the average COF by more than 15 %.

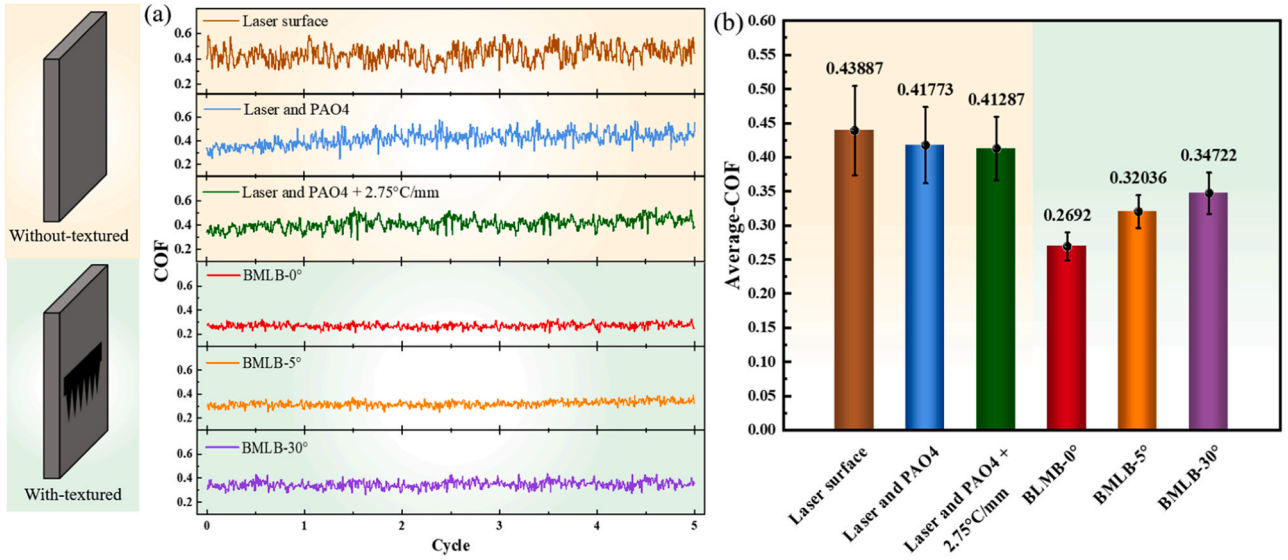


Fig. 6. Vertical friction test results (a) Without-textured and with-textured COF (b) Average COF.

Unlike the horizontal placement, vertical orientation of the sample significantly influences the motion of the lubricant due to gravity. The gravity effect leads to variations in the lubricant morphology across different textured surfaces, resulting in a pressure differential on both sides of the flow direction, thereby inducing lubricant migration and loss. The behavior of droplets on arbitrarily curved surfaces can be described using the Young–Laplace equation [44], which accounts for the Laplace pressure difference and gravity [45].

$$\Delta P = \gamma_{SL} \left( \frac{1}{R_1} + \frac{1}{R_2} \right) \quad (8)$$

$$R_1 = \frac{r}{\sin \theta_1}, R_2 = \frac{r}{\sin \theta_2} \quad (9)$$

$$\frac{dP}{dx} = -\frac{\Delta P}{L} + \rho g \sin \alpha \quad (10)$$

Here,  $\gamma_{SL}$  represents the surface tension of the liquid,  $R$  denotes the principal radius of curvature,  $\theta$  is the contact angle,  $\alpha$  is the inclination angle of the specimen, and  $\rho$  is the density of the lubricant. By incorporating the geometric parameters of the surface texture along with the physical properties of the lubricant. The velocity distribution along the direction of lubricant loss can be obtained by integrating the above equation.

$$v(y) = \frac{1}{2\nu} \left( -\frac{\Delta P}{L} + \rho g \sin \alpha \right) y(d - y) \quad (11)$$

Taking the average value of the integral, a predictive model for the lubricant loss rate can be established.

$$v_{avg} = \frac{1}{d} \int_0^d v(y) dy = \frac{1}{d} \cdot \frac{1}{2\nu} \left( -\frac{\Delta P}{L} + \rho g \sin \alpha \right) \cdot \frac{d^3}{6} \quad (12)$$

After simplification, the expression is as follows.

$$v_{loss} = \frac{\Delta P d^2}{12\mu L} \left( 1 - \frac{\rho g L^2 \sin \alpha}{2\Delta P} \right) \quad (13)$$

Where  $\Delta P$  denotes the pressure difference,  $d$  is the characteristic dimension at the texture tip,  $L$  represents the texture depth, and  $\mu$  is its viscosity. Based on these parameters, the lubricant loss volume  $V$  can be expressed as follows.

$$V_{loss} = A_{loss} \cdot h \quad (14)$$

Here,  $A_{loss}$  represents the area over which the lubricant spreads or is

lost on the surface, and  $h$  is the average thickness of the lubricant film, which is assumed to remain constant. Under the condition of a boundary length  $L$ , the lubricant loss area within a time period  $t$  can be expressed as:

$$A_{loss}(t) = \int_0^t Lv_{loss}(t') dt' \quad (15)$$

These results indicate that the lubricant loss area per unit time is proportional to the loss velocity. Therefore, under the same time interval, a higher lubricant loss rate corresponds to a larger spreading or depletion area, ultimately leading to a greater volume loss. As shown in Fig. 7(a)–(c), the downward lubricant loss area per second is visualized, and the quantitative analysis in Fig. 7(d) confirms that the BMLB-0° texture exhibits the smallest lubricant loss area and volume, whereas the BMLB-30° texture shows the largest loss in both area and volume. These findings demonstrate that fabricating the BMLB-0° texture on the sample surface effectively suppresses lubricant migration and loss, thereby enhancing friction reduction performance and achieving a lower COF. These results are consistent with the previously discussed tribological tests.

### 3.3. Application of surface textures

To evaluate the engineering applicability of the BMLB texture, a point-to-plane friction pair was adopted as the experimental configuration to simulate the operating conditions of bearings under low-speed and light-load conditions. A circumferential sliding friction and wear test was carried out on a ball-on-disk tribometer, as shown in Fig. 8(a). The upper specimen was a Si<sub>3</sub>N<sub>4</sub> ball with a diameter of 8 mm, and the lower specimen was an aluminum disk with a diameter of 40 mm and a thickness of 5 mm. A total of 5  $\mu$ L of PAO4 was used as the lubricant. The frictional radius was set to 10 mm, the rotational speed of the disk was 50 rpm, the test duration was 15 min, and the applied normal load was 1 N.

Based on previous research findings that texture orientation and geometric configuration influence lubricant migration [30,31], three texture types were further optimized and arranged into a continuous annular pattern. Textures were fabricated on laser-machined circular tracks with diameters of  $d_1 = 18.8$  mm and  $d_2 = 21.5$  mm, corresponding to centripetal (inner-ring side, Fig. 8(c)) and centrifugal (outer-ring side, Fig. 8(d)) orientations, respectively. The textured patterns were processed on aluminum circular specimens under identical laser parameters to assess the tribological performance of different texture



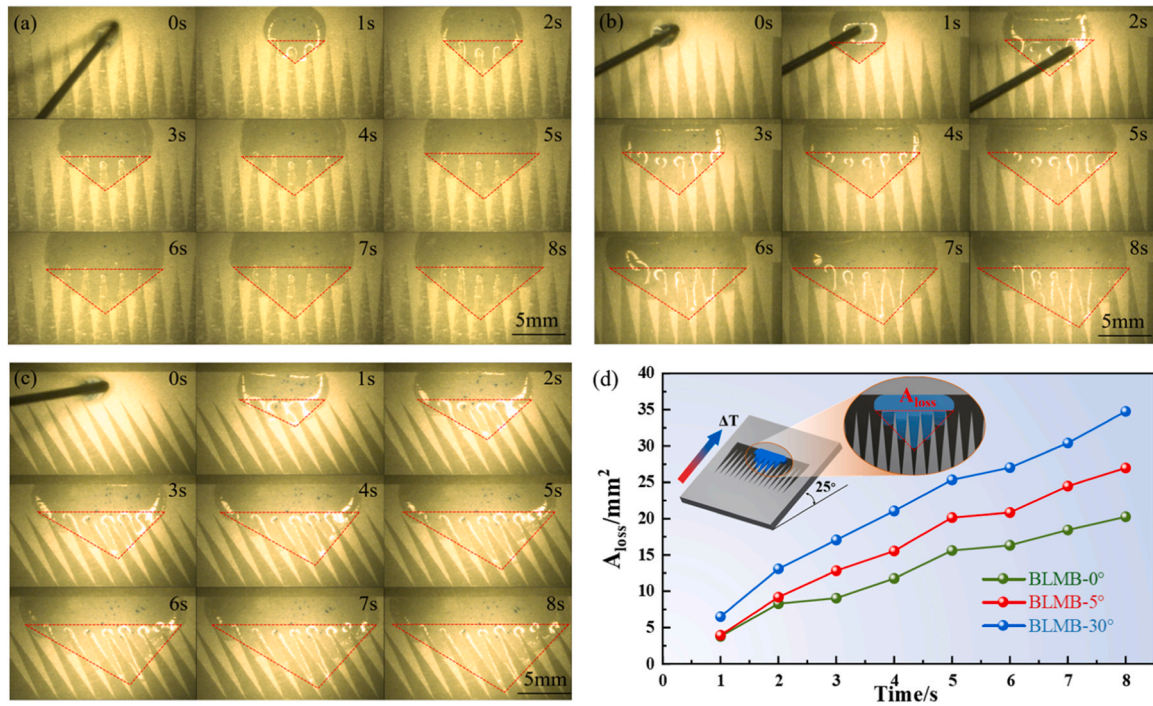


Fig. 7. Lubricant loss behavior on different textures (a) BMLB-0° (b) BMLB-5° (c) BMLB-30° (d) Area of lubricant loss.

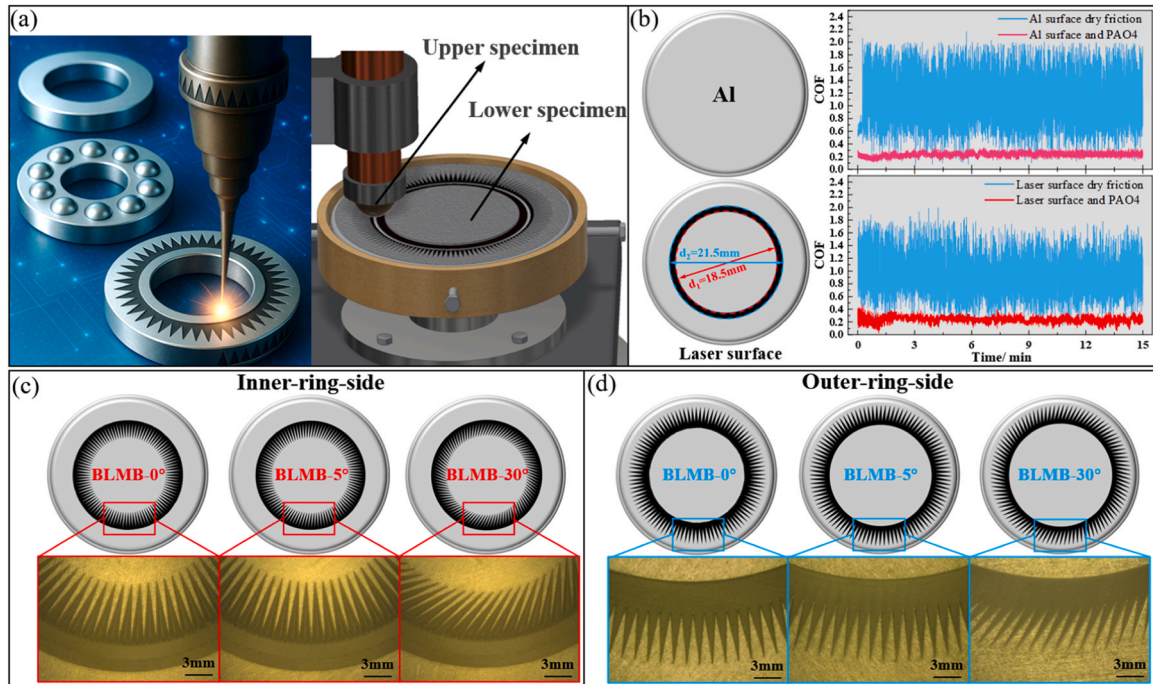


Fig. 8. (a) Ball-on-disk tribometer (b) Without-textured surface and frictional behavior (c) BMLB texture morphology of inner-ring-side (d) BMLB texture morphology of outer-ring-side.

arrangements under simulated conditions. The wear track width was observed using an ultra-depth-of-field optical microscope (VHX-600, China), and COF was calculated to quantify wear and evaluate the oil transport and friction-reducing performance of the BMLB texture.

By comparing the wear track widths in Fig. 9(d) and Fig. 10 (a) and the frictional behavior curves in Fig. 8(b) and Fig. 9(a) (b), it is observed that the aluminum surface and the laser surface with only a machined annular ring (without texture) exhibit the widest wear track widths and

highest COF under dry sliding conditions. The introduction of PAO4 lubrication significantly reduces both the wear scar width and COF. However, when centripetal textures are applied to the inner ring, the oil transport direction aligns with centrifugal force, accelerating lubricant loss. Consequently, the wear scar is slightly wider than that of the untextured surface, and the COF increases over time. In contrast, centrifugal textures on the outer ring promote oil retention by opposing the direction of centrifugal force, resulting in narrower wear scars and more



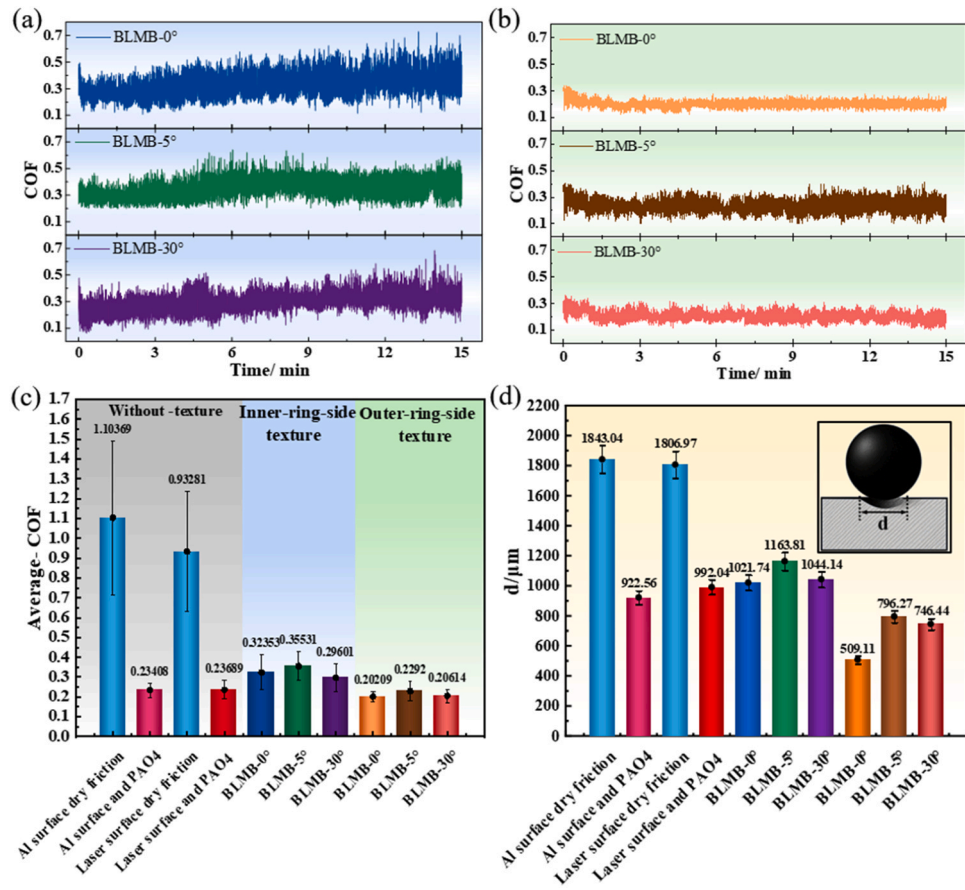


Fig. 9. Ball-on-disk friction test results (a) Inner-ring-side texture (b) Outer-ring-side texture (c) Average COF (d) Wear tracks width  $d$ .

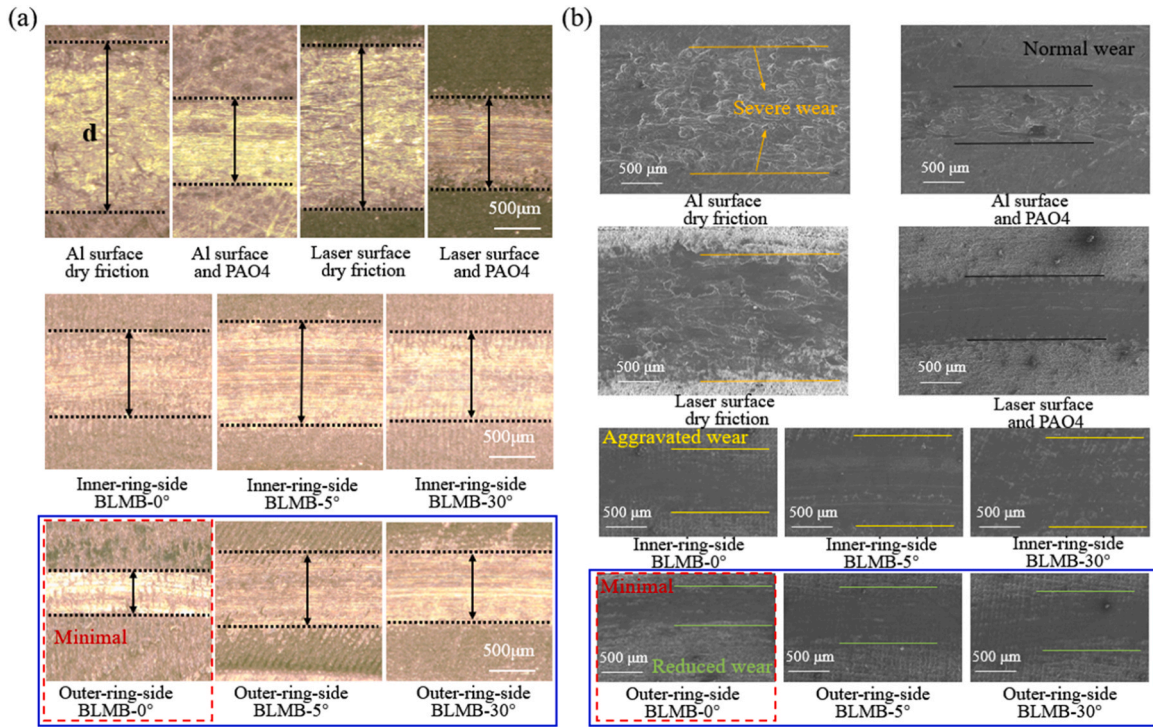


Fig. 10. (a) Wear tracks (b) SEM images of the wear.

stable COF curves. The BMLB-0° texture exhibits the narrowest wear scar and minimal COF fluctuation. As shown in Fig. 9(c), the centrifugal texture consistently maintains a lower and more stable COF compared to both centripetal textures and untextured surfaces under lubrication.

Further confirmation is provided by the SEM images of wear tracks in Fig. 10(b), which clearly show that the outer-ring-side texture effectively mitigates surface wear. The surface textured with the BMLB-0° configuration exhibited the least wear, demonstrating its superior anti-wear performance under lubricated conditions. These findings confirm that centrifugal texture alignment enhances oil retention and lubrication performance, whereas centripetal alignment exacerbates oil depletion and friction. They can reduce the average COF by more than 3 %. The wear track width can be reduced by up to 19 %. Among all configurations, the BMLB-0° centrifugal texture demonstrates the best overall tribological performance. It can reduce the average COF to 15 % compared to the aluminum surface. The wear track width is significantly reduced, with a maximum reduction of up to 48 %. These findings provide important theoretical support and optimization guidance for the surface texture design of rotating mechanical components such as bearings.

It should be noticed that although the tribological tests were conducted under light loading conditions, this investigation provides a proof-of-concept of a new means of migration-lubrication control under external thermal gradients for tribological pairs. As long as the texture remains structurally intact, it continues to exhibit friction-reducing effects even under increased loads. However, under excessive pressure conditions, issues such as edge collapse or localized fatigue wear may still occur.

#### 4. Conclusions

Inspired by the morphological characteristics of metasequoia leaves, this study develops a novel BMLB texture. Horizontal and vertical reciprocating friction tests are conducted to systematically investigate the lubrication regulation mechanisms of surface textures under the combined effects of gravity and thermal gradients. This study offers theoretical support and practical guidance for surface texture design in friction pairs under complex conditions, highlighting its promising application in lubrication enhancement of critical components such as aerospace bearings and precision linear guides. The main conclusions that can be drawn from this study are as follows:

1. Under horizontal reciprocating conditions (without gravity), the BMLB textures can reduce the average COF by over 31 %, of which the BMLB-5° has the best performance, and the reduction of average COF is 44 %.
2. Under vertical reciprocating conditions (with gravity), the BMLB textures exhibit over 15 % reduction in average COF, and significantly suppress frictional fluctuations and upward trends. Among all inclination angles, the BMLB-0° texture demonstrates best, achieving a 34 % reduction in average COF.
3. For the point-to-plane contact of the rotating pair, inducing the BMLB-0° texture can reduce the average COF by more than 15 %, and the wear track width is reduced by 48 %. Moreover, the frictional fluctuations can also be minimized.

#### Statement of originality

The submitted contents are original and not involving plagiarism with copyright infringement issues. I hereby declare and guarantee those are true, I claimed. I would like to declare on behalf of my co-authors that the work described was original research that has not been published previously, and not under consideration for publication elsewhere, in whole or in part.

#### CRedit authorship contribution statement

**Hao Qiu:** Writing – review & editing, Writing – original draft, Investigation, Formal analysis, Data curation. **Qingwen Dai:** Writing – review & editing, Funding acquisition, Conceptualization. **Wei Huang:** Supervision, Project administration, Methodology. **Xiaolei Wang:** Supervision, Project administration, Methodology.

#### Declaration of Competing Interest

The authors declare that they have no known competing financial interests or personal relationships that could have appeared to influence the work reported in this paper.

#### Acknowledgment

The authors thank the supported by National Key Laboratory of Helicopter Aeromechanics Funding, (2024-CXPT-GF-JJ-093-03) and the National Natural Science Foundation of China (Nos. 51805252 and 52175172).

#### Data Availability

Data will be made available on request.

#### References

- [1] Wang DW, Mo JL, Ouyang H, Chen GX, Zhu MH, Zhou ZR. Experimental and numerical studies of friction-induced vibration and noise and the effects of groove-textured surfaces. *Mech Syst Signal Process* 2014;46:191–208.
- [2] Grützmacher PG, Rosenkranz A, Rammacher S, Gachot C, Mücklich F. The influence of centrifugal forces on friction and wear in rotational sliding. *Tribol Int* 2017;116:256–63.
- [3] Karbalaeei A, Kumar R, Cho HJ. Thermocapillarity in microfluidics—A review. *Micromachines* 2016;7:13.
- [4] Grützmacher PG, Jalikop SV, Gachot C, Rosenkranz A. Thermocapillary lubricant migration on textured surfaces—a review of theoretical and experimental insights. *Surf Topogr Metrol Prop* 2021;9:013001.
- [5] Dai QW, Khonsari MM, Shen C, Huang W, Wang XL. Thermocapillary migration of liquid droplets induced by a unidirectional thermal gradient. *Langmuir* 2016;32:7485–92.
- [6] Dai QW, Huang W, Wang XL. Research process in mechanism and solution of liquid lubrication migration in space. *Surf Technol* 2014;43(6):125–30.
- [7] Dai QW, Huang W, Wang XL, Khonsari M. Directional interfacial motion of liquids: Fundamentals, evaluations, and manipulation strategies. *Tribol Int* 2021;154:106749.
- [8] Dai QW, Huang W, Wang XL. A surface texture design to obstruct the liquid migration induced by omnidirectional thermal gradients. *Langmuir* 2015;31:10154–60.
- [9] Grützmacher PG, Rosenkranz A, Szurdak A, Gachot C, Hirt G, Mücklich F. Lubricant migration on stainless steel induced by bio-inspired multi-scale surface patterns. *Mater Des* 2018;150:55–63.
- [10] Grützmacher PG, Rosenkranz A, Gachot C. How to guide lubricants—Tailored laser surface patterns on stainless steel. *Appl Surf Sci* 2016;370:59–66.
- [11] Liu Y, Chen JW, Zhang H, Gou HC, Dong GN. Wedge-shaped lyophilic pattern on superlyophobic surface for unidirectional liquid guidance and lubrication enhancement. *Tribology Int* 2024;194:109552.
- [12] Wang M, Liu Q, Zhang HR, Wang C, Wang L, Xiang BX, et al. Laser direct writing of tree-shaped hierarchical cones on a superhydrophobic film for high-efficiency water collection. *ACS Appl Mater Interfaces* 2017;9:29248–54.
- [13] Nakashima Y, Nakanishi Y, Yasuda T. Automatic droplet transportation on a plastic microfluidic device having wettability gradient surface. *Rev Sci Instrum* 2015;86.
- [14] Ghosh A, Ganguly R, Schutzius TM, Megaridis CM. Wettability patterning for high-rate, pumpless fluid transport on open, non-planar microfluidic platforms. *Lab a Chip* 2014;14:1538–50.
- [15] Dhiman S, Jayaprakash K, Iqbal R, Sen A. Self-transport and manipulation of aqueous droplets on oil-submerged diverging groove. *Langmuir* 2018;34:12359–68.
- [16] Feng W, Bhushan B. Multistep wettability gradient in bioinspired triangular patterns for water condensation and transport. *J Colloid Interface Sci* 2020;560:866–73.
- [17] Bliznyuk O, Jansen HP, Kooij ES, Zandvliet HJ, Poelsema B. Smart design of stripe-patterned gradient surfaces to control droplet motion. *Langmuir* 2011;27:11238–45.
- [18] Zheng YM, Bai H, Huang ZB, Tian XL, Nie F-Q, Zhao Y, et al. Directional water collection on wetted spider silk. *Nature* 2010;463:640–3.
- [19] Liu M, Wang S, Jiang L. Nature-inspired superwettability systems. *Nat Rev Mater* 2017;2:1–17.

- [20] Zhang C, Mcadams DA, Grunlan JC. Nano/micro-manufacturing of bioinspired materials: a review of methods to mimic natural structures. *Adv Mater* 2016;28: 6292–321.
- [21] Zhao WY, Zhang YL, Zhao XD, Ji ZY, Ma ZF, Gao XS, et al. Bioinspired design of a cartilage-like lubricated composite with mechanical robustness. *ACS Appl Mater Interfaces* 2022;14:9899–908.
- [22] Liu Y, Zhang H, Zhu Y, Chen JW, Wang P, Dai SJ, et al. Bionic jaw-like micro one-way valve for rapid and long-distance water droplet unidirectional spreading. *Nano Lett* 2023;23:5696–704.
- [23] Li J, Li JQ, Sun J, Feng SL, Wang ZK. Biological and engineered topological droplet rectifiers. *Adv Mater* 2019;31:1806501.
- [24] Ju J, Bai H, Zheng YM, Zhao TY, Fang R, Jiang L. A multi-structural and multi-functional integrated fog collection system in cactus. *Nat Commun* 2012;3:1247.
- [25] Guo L, Kumar S, Yang MY, Tang GH, Liu ZG. Role of the microridges on cactus spines. *Nanoscale* 2022;14:525–33.
- [26] Wu D, Wang JN, Wu SZ, Chen QD, Zhao S, Zhang H, et al. Three-level biomimetic rice-leaf surfaces with controllable anisotropic sliding. *Adv Funct Mater* 2011;21: 2927–32.
- [27] Long JY, Fan PX, Jiang DF, Han JP, Lin Y, Cai MY, et al. Anisotropic sliding of water droplets on the superhydrophobic surfaces with anisotropic groove-like micro/nano structures. *Adv Mater Interfaces* 2016;3:1600641.
- [28] Chen HW, Zhang PF, Zhang LW, Liu HL, Jiang Y, Zhang DY, et al. Continuous directional water transport on the peristome surface of *Nepenthes alata*. *Nature* 2016;532:85–9.
- [29] Zhang H, Dai SJ, Liu Y, Zhu YJ, Xu YD, Li BT, Dong GN. Fishbone-like micro-textured surface for unidirectional spreading of droplets and lubricity improvement. *Tribol Int* 2024;198:109932.
- [30] Chen SQ, Dai QW, Yang XL, Liu JJ, Huang W, Wang XL. Bioinspired functional structures for lubricant control at surfaces and interfaces: wedged-groove with oriented capillary patterns. *ACS Appl Mater Interfaces* 2022;14:42635–44.
- [31] Liu CL, Guo F, Wong P, Li XM. Laser pattern-induced unidirectional lubricant flow for lubrication track replenishment. *Friction* 2022;10:1234–44.
- [32] Vidyasagar KEC, Pandey RK, Kalyanasundaram D. Improvement of deep groove ball bearing's performance using a bionic textured inner race. *J Bionics Eng* 2021; 18:974–90.
- [33] Pattanayak MR, Pandey RK, Dutt JK. Performance improvement of an oil-lubricated journal bearing using bionic-textures fused micro-pockets. *J Tribology* 2022;144: 1–32.
- [34] Gouda B, Tandon N, Pandey RK, Babu CK. Comparison of fatigue life behavior between deep groove radial ball bearings possessing conventional and micro-grooved outer races operating under dry condition. *Proc Inst Mech Eng Part C J Mech Eng Sci* 2024;238:1671–87.
- [35] Gouda B, Tandon N, Pandey RK, Babu CK. Effect of grease grades on the tribological and vibrational behaviours of a radial ball bearing: conventional vs. micro-grooved outer races. *Proc Inst Mech Eng Part J J Eng Tribology* 2023;237: 300–17.
- [36] Gouda B, Tandon N, Pandey RK, Babu CK. Performance improvement of a radial ball bearing using a micro-groove on stationary outer race. *Proc Inst Mech Eng Part C J Mech Eng Sci* 2022;236:11521–36.
- [37] Gouda B, Tandon N, Pandey RK, Babu CK. Effects of positioning of inner race micro-textures on the tribodynamic performances of radial ball bearings. *Mech Syst Signal Process* 2025;223:111908.
- [38] Dai QW, Ji Y, Chong ZJ, Huang W, Wang XL. Manipulating thermocapillary migration via superoleophobic surfaces with wedge shaped superoleophilic grooves. *J Colloid Interface Sci* 2019;557:837–44.
- [39] Dumont B, Blau P, Crosbie G. Reciprocating friction and wear of two silicon nitride-based ceramics against type 316 stainless steel. *Wear* 2000;238:93–109.
- [40] Zhang AL, Li YX. Thermal conductivity of aluminum alloys—a review. *Materials* 2023;16:2972.
- [41] Scaraggi M. Lubrication of textured surfaces: a general theory for flow and shear stress factors. *Phys Rev E Stat Nonlinear Soft Matter Phys* 2012;86:026314.
- [42] Scaraggi M. Textured surface hydrodynamic lubrication: discussion. *Tribology Lett* 2012;48:375–91.
- [43] Gropper D, Wang L, Harvey TJ. Hydrodynamic lubrication of textured surfaces: a review of modeling techniques and key findings. *Tribol Int* 2016;94:509–29.
- [44] Siqveland LM, Skjaeveland SM. Derivations of the Young-Laplace equation. *Capillarity* 2021;4:23–30.
- [45] Décré MM, Baret J-C. Gravity-driven flows of viscous liquids over two-dimensional topographies. *J Fluid Mech* 2003;487:147–66.